

SUPPLEMENTAL MATERIAL: SPATIOTEMPORAL PATTERN FORMATION OF RHO GTPASES IN WOUND HEALING ON THE SURFACE OF A CELL

CORY M. SIMON^{A*}, EMILY M. VAUGHAN^B, WILLIAM M. BEMENT^B, LEAH EDELSTEIN-KESHET^A

^A The University of British Columbia. 121-1984 Mathematics Road, Vancouver, BC Canada V6T 1Z2

^B The University of Wisconsin, Madison

* CoryMSimon@gmail.com

CONTENTS

S1. Assumed uniformity of cytosolic protein concentrations	2
S2. Steps in model assembly	3
S3. The switch bifurcation	7
S4. The full model	8
S5. Parameter Estimation	9
S6. <i>In-silico</i> experiment details	10
S7. Two-wound simulations	10
S8. No-flux boundary condition derivation	12
S9. A change of variables to solve a moving boundary problem	12
S10. The numerical method	13
S11. Scaling the intensity data for comparison to simulations	13
References	13

S1. ASSUMED UNIFORMITY OF CYTOSOLIC PROTEIN CONCENTRATIONS

Here we justify several assumptions from considerations of diffusion and reaction time scales.

- *The bulk concentrations of Abr , $Cdc42$, and $RhoA$ in the cytosol are approximately constant throughout the wound healing process.* The band of RhoGTPase activity surrounding the wound is at most $30 \mu\text{m}$ thick, small by comparison to the oocyte diameter (around $1000 \mu\text{m}$). Around 1 % of RhoGTPases are active when a cell is in a resting state [1], and the activity is increased fourfold upon wounding only in the small region surrounding the wound. Thus, the increase in RhoGTPase activity in the wounded area has little effect on the total active RhoGTPase levels in the oocyte.
- *Spatial concentration gradients of the cytosolic proteins near the plasma membrane surface surrounding the wound are negligible.* The rate of diffusion of RhoGTPases in the cytosol is approximately 100 times that of the plasma membrane [2]. Inactive RhoGTPase recruited to the membrane and activated is replenished by diffusion on a fast time scale relative to the reaction rate at the plasma membrane. The reaction mean-free path (the average distance a molecule can travel before a collision that results in a reaction) is given by:

$$(1) \quad d_{rmfp} := \sqrt{D\tau_r},$$

for D the diffusion coefficient and τ_r the mean reaction time. As an example, for RhoA and parameter values in Table 2, $\tau_r \approx \frac{1}{(k_0^* + k_1)[R]} \approx 10$ s. Given a cytosolic diffusion rate of $10 \mu\text{m}^2/\text{s}$, we find that $d_{rmfp} \approx 10 \mu\text{m}$. Since the reaction mean-free path is on the order of the size of our domain, the approximation that the cytosolic species are spatially homogeneous [3] is reasonable.

S2. STEPS IN MODEL ASSEMBLY

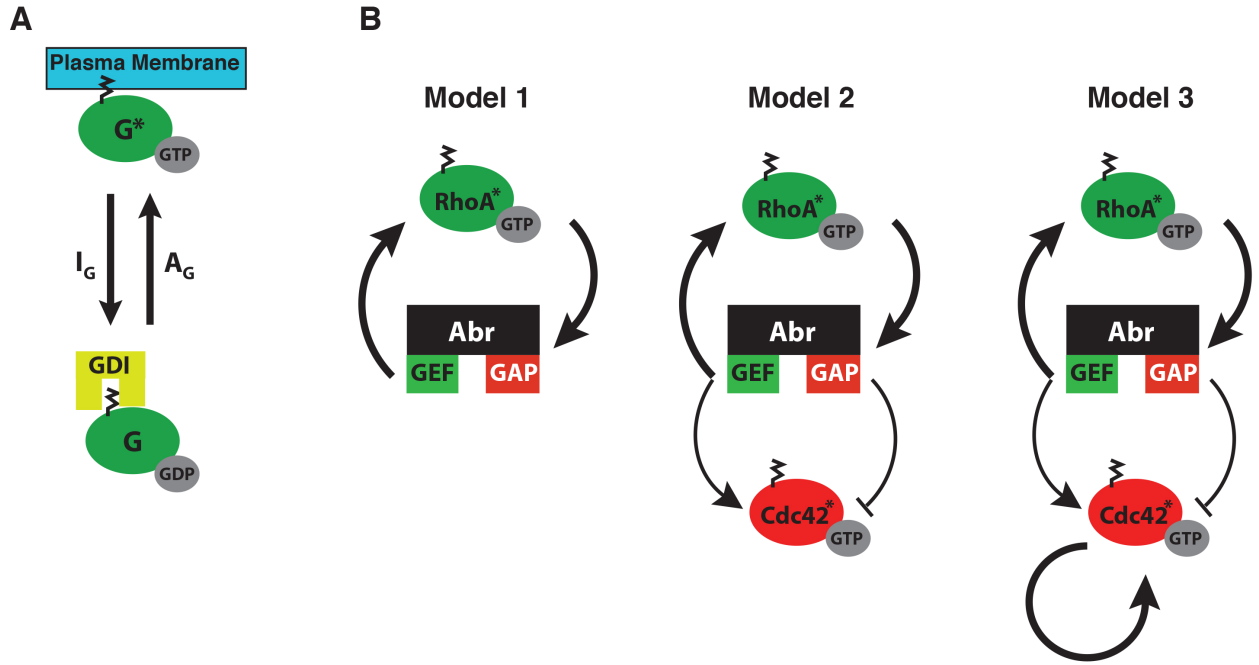


FIGURE S1. (a) Each RhoGTPase Cdc42 and RhoA is in flux on and off the membrane at rates A and I . The active forms (-GTP bound) are membrane bound. The GDIs (not explicitly modeled) are responsible for sequestering the GTPases in the cytosol. (b) The sequence of models leading us to the final model, where interactions are shown. Model 1 focuses on the RhoA-Abr module separately. Model 2 considers RhoA, Cdc42, and Abr, but lacks the positive feedback loop for Cdc42 that is in model 3.

The model was assembled in stages (Fig. S1) so as to test hypotheses about the interactions of the GTPases with each other and with Abr. This allows us to reject inappropriate variants before selecting a plausible candidate model that fits observations. We provide detail here. Using principles of parsimony and aiming to account for each basic experimental outcome, we first consider a spatially uniform scenario, and use simple linear and saturating kinetic terms (Michaelis-Menten and Hill functions). Based on the timescale of ≈ 1 min, we neglect protein synthesis of the GTPases and Abr.

We model the spatiotemporal concentration of the membrane bound species as defined in Table 1. All concentrations (in μM) at position x are total concentrations contained in a column of height dz and membrane surface area da , where, for simplification, we approximate the cell surface locally as flat and thickness, dz , as approximately constant. (See [4], Fig. 3 for a similar representation in a 2D cell simulation).

Models are tested for their ability to satisfy Properties 1 and 2 and those that fail are rejected. For completeness, we reiterate those properties here:

- Property 1: The experimentally known crosstalk scheme between RhoA, Abr, and Cdc42 (shown in Fig. 3B, model 2) is present in the reaction kinetics.
- Property 2: The combination of terms should allow for both low and high RhoGTPase levels. This implies the requirement for bistability (presence of two stable steady states). In the absence of a stimulus, cells are in a low GTPase-activity, stable, resting state.

As a reminder to the reader, the quantities $[R]$ and $[C]$ are taken as constants.

TABLE 1. Description of Quantities (PM is plasma membrane)

Variable	Description	Unit
$[R]$	Concentration of inactive RhoA in the cytosol	μM
$[R^*](r, t)$	Concentration of active RhoA anchored to the PM	μM
$[C]$	Concentration of inactive Cdc42 in the cytosol	μM
$[C^*](r, t)$	Concentration of active Cdc42 anchored to the PM	μM
$[AR^*](r, t)$	Concentration of Abr-bound active RhoA anchored to the PM	μM

S2.1. The RhoA and Abr Module Reaction Kinetics. Abr has a tight spatiotemporal correlation with active RhoA and, upon C3 exotransferase inhibition of RhoA, Abr recruitment was completely suppressed [5]. This suggests that active RhoA holds the primary responsibility for recruiting Abr to the membrane. We differentiate between active RhoA that is unbound or bound to Abr so that the total active RhoA on the surface at a point is $[R^*](r, t) + [AR^*](r, t)$.

S2.1.1. *Model 1a.* Our first model for active and Abr-bound active RhoA is

$$(2) \quad \begin{aligned} \frac{d[R^*]}{dt} &= (k_0^r + k_1[AR^*])[R] - k_2[R^*] - k_3[R^*], \\ \frac{d[AR^*]}{dt} &= k_3[R^*] - k_4[AR^*]. \end{aligned}$$

Here $k_3 = \hat{k}_3[A]$ for some \hat{k}_3 where $[A]$ is the cytosolic Abr concentration (not explicitly modeled). The term $k_3[R^*]$ is the rate at which binding occurs, $k_2[R^*]$ is loss of active RhoA through GAP-mediated inactivation and $k_4[AR^*]$ is rate of inactivation of Abr-bound active RhoA. About the rate of Rho activation, we took the linear form $A_{rho} = k_0^r + k_1[AR^*]$, where k_0^r is a basal rate of Rho activation due to other background GEF activity [6] and $k_1[AR^*]$ is an Abr-mediated GEF activation rate.

We solve for steady states of Eqs. 2 ($d[R^*]/dt = d[AR^*]/dt = 0$), represented by superscripts ^{SS}. We find that there is a single steady state

$$(3) \quad [R^*]^{SS} = \frac{k_4 k_0^r [R]}{k_4(k_2 + k_3) - k_1 k_3 [R]}.$$

From the fact that Model 1a has a unique steady state for $[R^*]$, it fails Property 2 and is rejected.

S2.1.2. *Model 1b.* We modified the model by assuming a saturating rate of Rho activation with respect to Abr

$$(4) \quad A_{rho} := k_0^r + \frac{k_1 [AR^*]^n}{K_A^n + [AR^*]^n}.$$

Then $n = 1$ corresponds to Michaelis-Menten kinetics, $n > 1$ to a Hill coefficient. Larger n correspond to sharper response. The model equations are then

$$(5) \quad \begin{aligned} \frac{d[R^*]}{dt} &= \left(k_0^r + \frac{k_1 [AR^*]^n}{K_A^n + [AR^*]^n} \right) [R] - k_2 [R^*] - k_3 [R^*], \\ \frac{d[AR^*]}{dt} &= k_3 [R^*] - k_4 [AR^*]. \end{aligned}$$

It is straightforward to show that $n \geq 2$ is required for bistability. This can be seen by plotting the curve that corresponds to $d[R^*]/dt = 0$ (the $[R^*]$ nullcline) together with the curve for $d[AR^*]/dt = 0$ (the $[AR^*]$ nullcline) in the $[R^*]$ - $[AR^*]$ plane (Fig. S2), and observing how these can intersect. For parameters in a suitable range, we find three intersections, two of which are the high and low stable steady state values of $[AR^*]$ and $[R^*]$ (Property 2). Regarding Property 1, once spatial terms are added, the form for A_{abr} allows for Abr to be locally recruited to regions where active RhoA is high. The GEF activity of Abr is modeled in A_{rho} . Thus, Property 1 and 2 are satisfied and we keep the model in Eqns. 5 for the RhoA-Abr module.

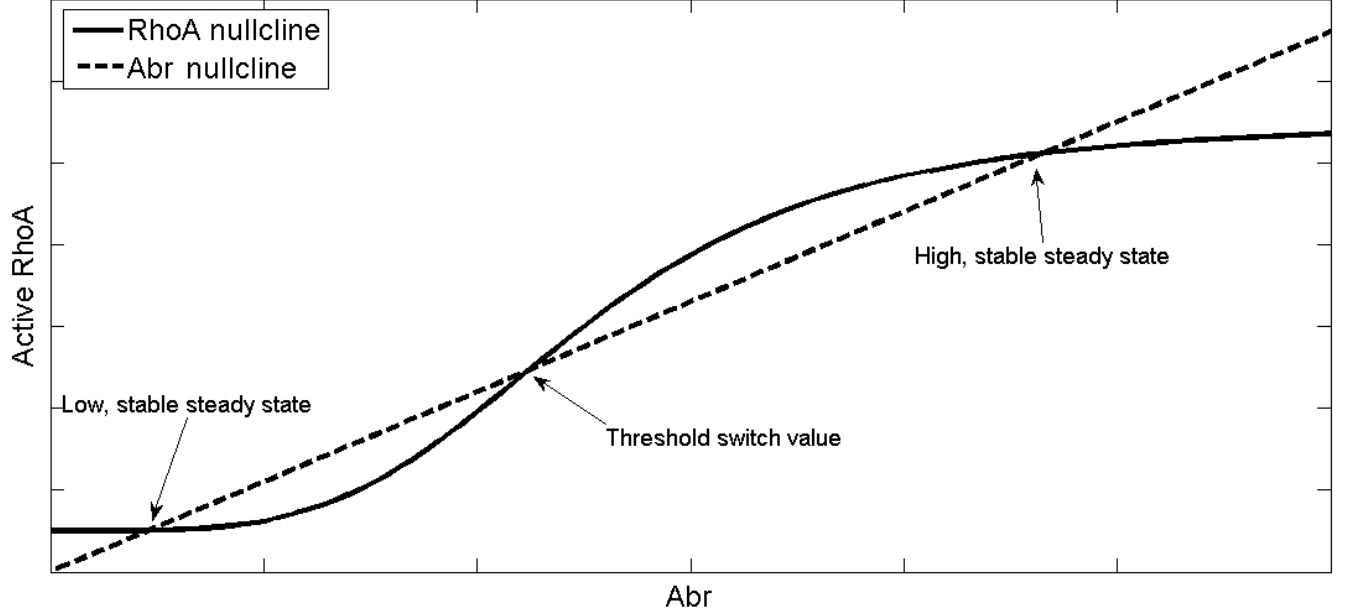


FIGURE S2. A caricature of RhoA and Abr nullclines of Eqns. 5. Each intersection of the nullclines is a steady state value. Both the high and low steady states have a basin of attraction, and either RhoA or Abr, or both, have to be pushed high enough to breach the separating border “threshold” (separatrix). Parameters are chosen in a way that gives realistic steady state values.

S2.2. The Cdc42 Module Reaction Kinetics. We next include Cdc42, which essentially reacts to the RhoA-Abr module.

S2.2.1. Model 2. As before, our default option is to consider linear GEF-mediated activation, $A_{cdc} = k_0^c + k_5[AR^*]$, where k_0^c is a basal level due to GEFs known to exist [6] aside from Abr. We also assume a linear inactivation rate $I_{cdc} := k_7 + k_8[AR^*]$, with k_7 the basal rate and $k_8[AR^*]$ the Abr-mediated rate. This leads to the equation

$$(6) \quad \frac{d[C^*]}{dt} = (k_0^c + k_5[AR^*])[C] - (k_7 + k_8[AR^*])[C^*],$$

whose steady state is,

$$(7) \quad [C^*]^{SS} = \frac{(k_0^c + k_5[AR^*])[C]}{k_7 + k_8[AR^*]}.$$

Recall that outside the RhoA zone, $[AR^*]$ is near its low, resting steady state value. However, Cdc42 activity can take on both low and high values. This is not possible for Eqn. 6, whose steady state is unique for a given value of $[AR^*]$, leading us to reject this model.

S2.2.2. Model 3a. Nonlinear kinetics in A_{cdc} or I_{cdc} as a function of $[AR^*]$ or $[R^*]$ will not suffice in generating the Cdc42 pattern since both a high and low level of Cdc42 activity are maintained outside of the RhoA zone where $[AR^*]$ is at a constant value. We therefore consider a form of Cdc42 autocatalysis, where A_{cdc} is an increasing function of $[C^*]$. We first test a linear autocatalysis term:

$$(8) \quad \frac{d[C^*]}{dt} = (k_0^c + k_5[AR^*] + k_6[C^*])[C] - (k_7 + k_8[AR^*])[C^*].$$

We find that the steady state

$$(9) \quad [C^*]^{SS} = \frac{(k_0^{cdc} + k_5[AR^*])[C]}{k_7 + k_8[AR^*] - k_6[C^*]},$$

is unique for a given $[AR^*]$, and, as before, we reject this variant of positive feedback.

S2.2.3. *Model 3b.* We finally adopt a saturating Hill-function term for the Cdc42 positive feedback, with the equation

$$(10) \quad \frac{d[C^*]}{dt} = \left(k_0^c + k_5[AR^*] + \frac{k_6[C^*]^n}{K_C^n + [C^*]^n} \right) [C] - (k_7 + k_8[AR^*])[C^*].$$

It is straightforward to show that for a given $[AR^*]$ level and suitable parameter ranges, this equation exhibits bistability. Thus, Cdc42 can have both high and low levels close to and far from the wound, respectively (Property 2). We have also included all known interactions between RhoA, Cdc42, and Abr (Property 1). This is the simplest model of the type capable of exhibiting Properties 1 and 2.

S3. THE SWITCH BIFURCATION

Fig. S3 shows a sketch of the bifurcation diagram for the well-mixed system with respect to the parameter k_0^r . The solid curves represent stable steady states, and the dashed curve is an unstable steady state that forms a threshold for stimuli that can “flip the switch” between the two steady states [7]. For a parameter range, there are two stable steady states (bistability). The bifurcation diagram was created by setting the kinetics for $[R^*]$ and $[AR^*]$ in the differential Eqns. 5 to zero and solving the nonlinear system with Newton’s method as the parameter k_0^r changes in a loop. All three branches are found by choosing a suitably close initial guess in the Newton solver inside the loop.

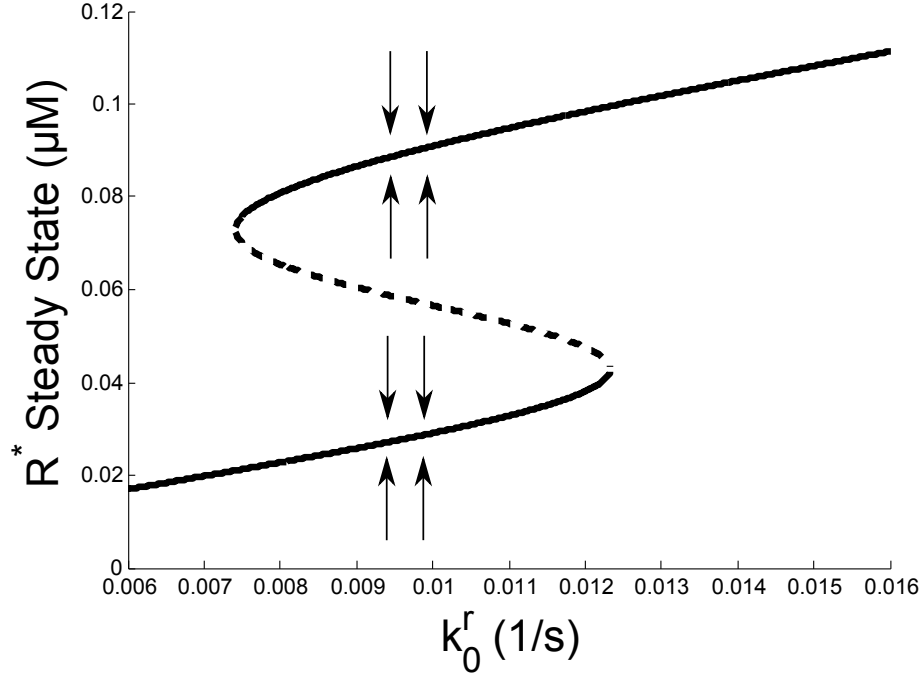


FIGURE S3. Bifurcation diagram for active RhoA with respect to k_0^r for the well-mixed system in Eqns. 5. The bottom (top) solid curve is the low (high), stable steady state curve. The middle dashed curve is the unstable steady state. The arrows indicate which steady state is attained from various initial values of $[R^*]$.

We include the spatial terms that model diffusion and advection due to the myosin-powered movement inward toward the wound:

$$(11) \quad \frac{\partial[G]}{\partial t} = \nabla \cdot (D\nabla[G] - \mathbf{v}[G]) + \text{reaction},$$

where D is the diffusion coefficient and \mathbf{v} is the advection velocity vector. With the reaction terms from the well-mixed system outlined above, we can think of a reaction-diffusion-advection system as governed by the switch bifurcation in Fig. S3 whose behavior is determined *locally* in space. In fact, a reaction diffusion equation can be simulated as several well-mixed spatial compartments where molecules move between compartments due to diffusion [8]. Thus, in a particular compartment that obeys the well-mixed kinetics we analyzed here, if the concentration of RhoA is below [above] the threshold (dashed line), the concentration will have a tendency to move to the low [high] steady state. This is the essence of ‘spatial bistability’, where the state that the system is attracted to depends on the spatial location in question.

S4. THE FULL MODEL

The full final model to be simulated is

$$\begin{aligned}\frac{\partial[AR^*]}{\partial t} &= \nabla \cdot (D\nabla[AR^*] - \mathbf{v}[AR^*]) + k_3[R^*] - k_4[AR^*], \\ \frac{\partial[R^*]}{\partial t} &= \nabla \cdot (D\nabla[R^*] - \mathbf{v}[R^*]) + \left(k_0^r + \frac{k_1[AR^*]^n}{K_A^n + [AR^*]^n} \right) [R] - k_2[R^*] - k_3[R^*], \\ \frac{\partial[C^*]}{\partial t} &= \nabla \cdot (D\nabla[C^*] - \mathbf{v}[C^*]) + \left(k_0^c + k_5[AR^*] + \frac{k_6[C^*]^n}{K_C^n + [C^*]^n} \right) [C] - (k_7 + k_8[AR^*])[C^*],\end{aligned}$$

where, under our assumption of radial symmetry, the spatial effects of diffusion and advection can be written as:

$$(12) \quad \nabla \cdot (D\nabla[G] - \mathbf{v}[G]) = \frac{1}{r} \frac{\partial}{\partial r} \left(rD \frac{\partial[G]}{\partial r} + rv[G] \right).$$

We assume no-flux boundary conditions at the wound edge, and a basal steady state level far away from the wound, that is

$$\begin{aligned}\frac{\partial[AR^*]}{\partial r} = \frac{\partial[R^*]}{\partial r} = \frac{\partial[C^*]}{\partial r} &= 0 \text{ at } r = w(t), \\ [AR^*] = [R^*] = [C^*] &= \text{low, stable steady state values for } r \rightarrow \infty.\end{aligned}$$

(See also Section S8).

As the wound edge closes, it advects the membrane inwards. The advection velocity has only an inward radial component $v_r(r)$. The equation of continuity on the plane is $\frac{1}{r} \frac{\partial}{\partial r} (rv_r) = 0$ and implies that $v_r = \frac{v_c}{r}$ for some constant v_c (which may be a function of time). We choose the v_c such that the wound location data matches the simulated wound location at the final time of simulation since the rate of wound closure drives the advection. The velocity of the moving boundary is assumed to be $w'(t) = -v(w(t))$. More precisely, as the wound edge closes, it advects the membrane inwards. Data for the advection velocity as a function of distance from the wound is found in [9], but 3D effects are here, such as curvature effects and the z-ward ingression of the membrane. Despite this, the profile appears to fit a $\frac{1}{r}$ dependence in [9].

The initial conditions for active RhoA ($[AR^*] + [R^*]$) and active Cdc42 are triangular-shaped peaks that correspond to the intensity data at 48 seconds after wounding.

S5. PARAMETER ESTIMATION

TABLE 2. Parameters: + denotes ‘constrained via steady state values’

Parameter	Interpretation	Value	Unit	Source
k_0^r	Basal RhoA activation	0.009	s^{-1}	+ [10, 11, 1]
k_0^c	Basal Cdc42 activation	0.0015	s^{-1}	+ [10, 11, 1]
k_1	Maximum GEF activity of Abr on RhoA	0.0232	s^{-1}	+ [10, 11, 1]
K_A	Measure of switch location in Hill eqn.	0.0082	μM	intensity data
K_C	Measure of switch location in Hill eqn.	0.0546	μM	intensity data
k_2	GAP /GDI inactivation rate of RhoA	1	s^{-1}	[10]
k_3	Abr binding rate to RhoA	0.1	s^{-1}	
k_4	GAP /GDI inactivation rate of Abr-RhoA	6/9	s^{-1}	[10, 12]
k_5	Abr GEF activity on Cdc42	1.2987	s^{-1}	intensity data
k_6	Maximum autocatalysis rate of Cdc42	0.0312	s^{-1}	+ [10, 11, 1]
k_7	Background GAP /GDI inactivation rate of Cdc42	0.4741	s^{-1}	[10]
k_8	Abr GAP activity on Cdc42	127.3926	s^{-1}	intensity data
v_c	Advection velocity parameter	1.1179	$\mu\text{m}^2/\text{s}$	wound location data
n	Hill Coefficient	6		

The following parameters provide rough estimates. At present, the model is qualitative rather than quantitatively precise. According to [10] based on data in [11] for fibroblasts, there is typically $3.1 \mu\text{M}$ RhoA and $2.4 \mu\text{M}$ Cdc42 in a cell. According to [1], around 1% of total RhoGTPase is in the active form in a resting cell. Hence, we use $[R] = 3.1 \mu\text{M}$ and $[C] = 2.4 \mu\text{M}$ and choose the parameter regime such that the low, basal steady state value of $[R^*] + [AR^*]$ and $[C^*]$ is $0.03 \mu\text{M}$ and $0.02 \mu\text{M}$, respectively. Upon wounding, local Cdc42 and RhoA activity increases by 200-800%, and here we used a four-fold factor. Hence we identified a parameter regime that yields $([R^*] + [AR^*])_{low}^{SS} = 0.03 \mu\text{M}$, $([R^*] + [AR^*])_{high}^{SS} = 0.1 \mu\text{M}$, $[C^*]_{low}^{SS} = 0.02 \mu\text{M}$, and $[C^*]_{high}^{SS} = 0.1 \mu\text{M}$. In achieving these high and low steady-states, the parameters K_A and K_C are constrained to lie in a particular interval (explaining * in Table 2). See Fig. S2 for an interpretation of the high and low steady state values.

The membrane diffusion coefficient D is taken to be $0.1 \mu\text{m}^2/\text{s}$ [2]. According to [13], the rate of GTP hydrolysis of RhoA by GAP has been measured as 1.5 s^{-1} (similar to measurements reported in [14]), and coupled with GDI sequestration rates, we take the GAP deactivation rate $k_2 = k_7 + k_8[AR^*]_{low}^{SS} = 1 \text{ s}^{-1}$ as in [10]. Abr inhibits GTP dissociation in GTPases, and from Fig. 2 in [12], we estimate $k_4 = \frac{2}{3}k_2$.

To obtain the appropriate estimated levels of observed high and low GTPase activity levels, we constrained the parameters k_0^r , k_1 for RhoA, and $k_0^{effective} := k_0^c + k_5[AR^*]_{low}^{SS}$ and k_6 for Cdc42. The parameter $k_0^{effective}$ represents basal Cdc42 rate of activation away from the wound.

The radial advection velocity of the membrane fluid is $v_r(r) = \frac{v_c}{r}$, and v_c is chosen to yield a simulated wound location that matches the wound location in the data at $t = 30 \text{ s}$ simulation time.

The parameters K_C and K_A determine the threshold concentration that must be breached in order to locally switch the system into a high steady state from the basal state. Taking the initial condition from the intensity data, we include these parameters that determine the threshold in the optimization routine that fits the simulated profiles to the intensity data. To allow for a robust range of values that maintains the bistable property, we used the Hill coefficient $n = 6$. ($n = 2$ works in a narrower range of parameters). Parameters k_2 , k_4 , and $k_7 + k_8[AR^*]_{low}^{SS}$ are constrained by typical steady-state GTP hydrolysis rates, leaving the parameters k_3 , k_5 , and k_8 , K_A , and K_C free. A least-squares nonlinear, constrained optimization routine in MATLAB (fmincon) is used to fit the simulated concentration profiles to the intensity data at $t = 30$ using the threshold parameters K_A and K_C as well as k_3 , k_5 . We set the ratio of $\frac{k_5}{k_8} \approx 0.01$ to determine k_8 based on k_5 in order to observe the low levels of Cdc42 inside the Rho zone and obtain a fit.

S6. *In-silico* EXPERIMENT DETAILS

In each scenario, altering Abr has an effect, albeit a small one, on the background levels of the GTPases. Thus, in each case, we recalculate the background levels $[R^*]_{low}^{SS}$, $[AR^*]_{low}^{SS}$ and $[C^*]_{low}^{SS}$ and recalculate the resting inactive global concentrations $[R]$ and $[C]$, which are treated as constants. This calculation is done by assuming that the total amount of GTPase (active+inactive) in the cell is constant throughout the wounding process and mutant protein overexpressions.

S6.1. Validation: Wild Type Abr Overexpression. We mimicked this manipulation of wildtype Abr overexpression *in silico* by increasing the value of k_3 in which the cytosolic concentration of Abr is embedded in the mass action of RhoA-cytosolic Abr binding term (equivalent to increasing $[A]$). Increasing k_3 by 20 %, the Rho zone widens significantly and overtakes the Cdc42 zone, and high levels of Cdc42 are not observed (Fig. 6). This can be understood from the fact that Abr microinjection results in a drop in the threshold value for Rho (Fig. 7). The Cdc42 activation-inactivation curves show that the Cdc42 zone is less intense with more cytosolic Abr. As the Rho zone broadens, it overtakes the Cdc42 zone with its high levels of Abr, suppressing the Cdc42 zone to its lower stable steady state that remains. With more extreme changes in k_3 , the Rho-Abr module loses bistability and only a high steady state remains as the positive feedback from the Abr is too strong to maintain a low steady state. The parameter k_3 can be increased by a factor of 1.22 before the Rho-Abr module becomes mono-stable at a high steady state.

S6.2. Validation: overexpression of GEF-dead Abr. Here, we model the GEF-dead Abr domain by decreasing k_1 and k_5 to 30 % of controls and model the overexpression of Abr by increasing k_3 by 20 %. Neither the RhoA nor Cdc42 zone can be sustained (Fig. 6B) because the model loses bistability for both RhoA and Cdc42 under these parameter changes, and only the low steady states remain (Fig. 7).

S6.3. Validation: overexpression of GAP-dead Abr. The effects of GAP-dead Abr expression were represented by decreasing k_8 to 75 % of its original value and increasing k_3 by 20 % to represent the overexpression of Abr. As shown in Fig. 6C, zones overlap and broaden in comparison to controls. The bottom panel shows that the threshold switch value for RhoA and Cdc42 are both lower than in controls, resulting in the broadening of the zones given the same height stimulus as in the control simulation. Beyond a certain level of GAP-dead Abr overexpression, the RhoA-Abr nullclines have only one intersection, resulting in only one high steady state for RhoA (same as WT Abr overexpression for the RhoA-Abr module). Furthermore, as k_8 decreases and k_3 increases, the intersections of the rates of activation and inactivation of Cdc42 result in only one high steady state due to the increasing GEF activity of the Abr. However, for this modest decrease in k_8 and increase in k_3 , the model is capable of capturing the experimental result [5] that both zones broaden. we have assumed in our model.

S6.4. Validation: C3 exotransferase inhibited RhoA. The effects of C3 were represented by setting the RhoA activation terms k_0^r and k_1 to be 30 % of their values in the control simulation. The simulation results are in Fig. 6D. The bottom panel shows that the RhoA nullcline is translocated downwards and scaled, resulting in only one stable steady state for RhoA. Without much active RhoA, there is very little Abr and the Cdc42 rates of inactivation and activation intersect in different places. Specifically, the low steady state is lower and the high steady state is higher, resulting in a more intense zone as in experiments [15]. Even though the threshold value during the inhibition of RhoA in our model is not significantly different from the controls, our model still captures the broadening of the Cdc42 zone that was observed in experiments [15] simply because the Rho zone is no longer present to suppress it in that region.

S7. TWO-WOUND SIMULATIONS

Here we consider the case of two wounds whose edges are a distance L apart. We ask how pattern dynamics depend on L . We ignore the effects of advection and wound closure, and simulate Model 3 in two dimensions by triangulating the geometry and using a finite volume method in a Python package FiPy [16]. For $G = \text{Abr}$, Rho, and Cdc42, the evolution of the concentrations is governed by the reaction-diffusion equations:

$$\begin{aligned} \frac{\partial[G]}{\partial t} &= D\Delta[G] + f_G(\{[G_k]\}) \text{ for } x \in \Omega, t > 0, \\ \frac{\partial[G]}{\partial n} &= 0 \text{ in } \partial\Omega, \end{aligned}$$

where Ω is the swiss-cheese shaped region from the two wounds and n is the outward normal vector to the boundary. As before, we impose no flux boundary conditions at the wound edge. The no flux boundary condition in the far field is used as an approximation. The kinetics functions and parameter values are taken directly from our default single-wound simulations. The initial stimuli at each wound are similar to the 1D

simulations, but were slightly modified to qualitatively yield a Rho and Cdc42 zone in a single-wound scenario. By approximating the system by neglecting advection, closure of the wound, and Diriclet BCs, a different initial condition was required to yield the same qualitative behavior as the simulations in Fig 5C. Between the wounds, we assume that the stimuli are additive when they spatially overlap. If the wounds are close, the stimuli will overlap. If they are far away, the stimuli do not overlap.

S8. NO-FLUX BOUNDARY CONDITION DERIVATION

Here, we derive the no flux boundary condition at the wound edge, which is complicated by the moving boundary. Intuitively, the boundary is moving at the same rate as the advection at the wound edge, so the end result should be that the radial derivative is zero at the wound edge. Let $u(r, t)$ be the concentration of one of the proteins. Consider the radial axis as the top-down view of the surface of the cell with the wound at the center. We have the wound location as $r = w(t)$ and it changes with time according to $w'(t) = -v(w(t))$, where $v(r)$ is the velocity towards the wound center. The conservation equation governing each species u that is attached to the membrane is:

$$(13) \quad \frac{\partial u}{\partial t} = \frac{1}{r} \frac{\partial}{\partial r} \left(rD \frac{\partial u}{\partial r} + rvu \right) + f(u).$$

The reaction term $f(u)$ will also depend on other chemical species, but the extension to multiple species is trivial. We use the Rankine-Hugoniot jump condition [17] to have no flux across the wound edge by defining $u(r, t) \equiv 0$ for $0 \leq r < w(t)$ and treating the wound edge as a moving discontinuity. Integrating Eqn. 13 over the spatial domain $r_1 < w(t) < r_2$, we have:

$$(14) \quad 2\pi \frac{\partial}{\partial t} \int_{r_1}^{r_2} r u dr = 2\pi \int_{r_1}^{r_2} \frac{\partial}{\partial r} \left(rD \frac{\partial u}{\partial r} + rvu \right) dr + 2\pi \int_{r_1}^{r_2} r f(u) dr$$

Splitting the integral on the left into two and evaluating the first integral on the right:

$$(15) \quad \frac{\partial}{\partial t} \left(\int_{r_1}^{w(t)} r u dr - \int_{r_2}^{w(t)} r u dr \right) = \left(rD \frac{\partial u}{\partial r} + rvu \right) \Big|_{r_1}^{r_2} + \int_{r_1}^{r_2} r f(u) dr$$

Accounting for zero amount of u in $0 \leq r < w(t)$, this integration reduces to:

$$(16) \quad - \int_{r_2}^{w(t)} r u_t dr - w(t)w'(t)u \Big|_{w(t)} = Dr_2 \frac{\partial u}{\partial r} \Big|_{r_2} + r_2 v u \Big|_{r_2} + \int_{r_1}^{r_2} r f(u) dr.$$

Finally, we take the limit as $r_1 \rightarrow w(t)^-$ and $r_2 \rightarrow w(t)^+$, causing the integral of the reaction term and the first integral above on the left hand side to vanish since the integration is over an empty interval. Using $w'(t) = -v(w(t))$, we arrive at our no flux boundary condition:

$$(17) \quad w(t)v u \Big|_{w(t)} = Dw(t) \frac{\partial u}{\partial r} \Big|_{w(t)} + w(t)v u \Big|_{w(t)},$$

or $\frac{\partial u}{\partial r} = 0$ at $r = w(t)$.

S9. A CHANGE OF VARIABLES TO SOLVE A MOVING BOUNDARY PROBLEM

The coupled reaction-diffusion-advection system contains a moving boundary that is treated as stationary using a coordinate transformation. Far away from the wound, which we treat as a far field, we have that the proteins are at their basal, low steady state values, $u(\infty, t) = u^{SS}$. At the wound edge $r = w(t)$, we have no-flux boundary conditions. We change from a moving coordinate to a fixed coordinate by the transformation

$$(18) \quad \psi(r, t) := r - w(t)$$

so that $r = w(t)$ corresponds to $\psi = 0$ and we still have a far-field in ψ . ψ is the shortest distance of a point on the surface to the wound boundary. This change of coordinates leads to a fixed coordinate system. By the chain rule:

$$(19) \quad \frac{\partial}{\partial t} = \frac{\partial}{\partial t} + \frac{\partial \psi}{\partial t} \frac{\partial}{\partial \psi}, \quad \frac{\partial}{\partial r} = \frac{\partial \psi}{\partial r} \frac{\partial}{\partial \psi}$$

and Eqn. 18 gives that $\frac{\partial \psi}{\partial t} = -w'(t)$.

In rewriting Eqn. 13 in terms of the the radial coordinate with the function form of the velocity as $v_r(r) = \frac{v_c}{r}$, we get

$$(20) \quad \frac{\partial u}{\partial t} = \frac{1}{r} \frac{\partial}{\partial r} \left(rD \frac{\partial u}{\partial r} + v_c u \right) + f(u),$$

and transform into the new variables (ψ, t) , to get a PDE for $\hat{u}(\psi, t)$:

$$(21) \quad \begin{aligned} \frac{\partial \hat{u}}{\partial t} &= D \frac{\partial^2 \hat{u}}{\partial \psi^2} + \frac{\partial \hat{u}}{\partial \psi} \left(w'(t) + \frac{D + v_c}{\psi + w(t)} \right) + f(\hat{u}), \\ \frac{\partial \hat{u}}{\partial \psi}(0, t) &= 0, \quad \hat{u}(\infty, t) = u^{SS}. \end{aligned}$$

This characterizes a system on the static ψ domain. For plotting purposes, after the above system is solved, we can plot in the r coordinates using $r = \psi + w(t)$.

S10. THE NUMERICAL METHOD

Finite difference methods are used to solve the PDE system. The Laplacian operator is treated implicitly in time, upwinding is used for the advection terms, and the reaction terms are treated explicitly. We approximate the far field by $\psi = 50 \mu\text{m}$, a large distance from the wound. Given a set of parameter values, we solve for the steady states and set the far-field condition as the low steady state G_{low}^{SS} solution. At each time step, we compute v according to its prescription, and then update the position of the moving boundary using $w'(t) = -v(w(t))$. Upon resolving each the spatial and temporal time steps, we find no significant distinction between solutions. We use MATLAB for all simulations, except for the FiPy package in FiPy that is used for the two-dimensional simulations of two wounds.

Details: let u_j^k be the approximation to $\hat{u}(\psi_j, t_k)$ for $t_k := k\Delta t$ and $\psi_j := j\Delta\psi$ where Δt and $\Delta\psi$ are the time and spatial steps, respectively. Our discretization scheme is then:

$$(22) \quad \frac{u_j^{k+1} - u_j^k}{\Delta t} = D \frac{u_{j-1}^{k+1} - 2u_j^{k+1} + u_{j+1}^{k+1}}{(\Delta\psi)^2} + \frac{u_{j+1}^{k+1} - u_j^{k+1}}{\Delta\psi} \left(\frac{v_c + D}{\psi_j + w(t_k)} + w'(t_k) \right).$$

Handling of the boundary conditions: no flux $\implies u_{-1} = u_1$. Dirichlet condition the far field $\implies u_N = u^{SS}$ where ψ_N is the truncation location for approximation of the far-field.

S11. SCALING THE INTENSITY DATA FOR COMPARISON TO SIMULATIONS

From each intensity point, we first subtract the background level, which we take as the average over time of the intensity at the pixel value furthest from the wound. We then scale the RhoA intensity by the amplitude of $[R^*]_{high}^{SS} + [AR^*]_{high}^{SS} - ([R^*]_{low}^{SS} + [AR^*]_{low}^{SS})$ and adding $[R^*]_{low}^{SS} + [AR^*]_{low}^{SS}$ to it to adjust for the background levels. We scale the Cdc42 intensity by $[C^*]_{high}^{SS} - [C^*]_{low}^{SS}$ and add $[C^*]_{low}^{SS}$ to it to adjust for the background levels.

REFERENCES

- [1] E. Boulter, R. Garcia-Mata, C. Guilly, A. Dubash, G. Rossi, P. Brennwald, and K. Burridge. Regulation of RhoGTPase crosstalk, degradation and activity by RhoGDI1. *Nature Cell Biology*, 12:477, 2010.
- [2] M. Postma, L. Bosgraaf, H. Looers, and P. Van Haastert. Chemotaxis: signalling modules join hands at front and tail. *EMBO reports*, 5:35–40, 2004.
- [3] R. Grima and S. Schnell. Modeling reaction kinetics inside cells. *Essays in Biochemistry*, 45(3):41–56, 2008.
- [4] A. Mareć, A. Jilkin, A. Dawes, V. Grieneisen, and L. Edelstein-Keshet. Polarization and Movement of Keratocytes: A Multiscale Modelling Approach. *Bulletin of Mathematical Biology*, 68:11691211, 2006.
- [5] E. Vaughan, A. Miller, H. Yu, and W. Bement. Control of Local Rho GTPase Crosstalk by Abr. *Current Biology*, 21:1–8, 2011.
- [6] O. Pertz. Spatio-temporal Rho GTPase signaling: where are we now? *Journal of Cell Science*, 123:1841–1850, 2010.
- [7] J. Tyson, K. Chen, and B. Novak. Sniffers, buzzers, toggles and blinkers: dynamics of regulators and signaling pathways in the cell. *Current Opinion in Cell Biology*, 15:221–231, 2003.
- [8] R. Erban, S. Chapman, and P. Maini. A practical guide to stochastic simulations of reaction-diffusion processes. URL: people.maths.ox.ac.uk/~erban/Education/StochReacDiff.pdf.
- [9] C. Mandato and W. Bement. Contraction and polymerization cooperate to assemble and close actomyosin rings around Xenopus oocyte wounds. *Journal of Cell Biology*, 154(4):785–797, 2001.
- [10] A. Jilkin, A. Maree, and L. Edelstein-Keshet. Mathematical Model for Spatial Segregation of the Rho-Family GTPases Based on Inhibitory Crosstalk. *Bulletin of Mathematical Biology*, 2007.
- [11] D. Michaelson, J. Silletti, G. Murphy, P. D. Eustachio, M. Rush, and M. Philips. Differential Localization of Rho GTPases in Live Cells: Regulation by Hypervariable Regions and RhoGDI Binding. *Journal of Cell Biology*, 152(1):111–126, 2001.

- [12] T. Chuang, X. Xu, V. Kaartinen, N. Heisterkamp, J. Groffen, and G. Bokoch. Abr and Bcr are multifunctional regulators of the Rho GTP-binding protein family. *Proceedings of the National Academy of Sciences*, 92:10282–10286, 1995.
- [13] B. Zhang and Y. Zheng. Regulation of RhoA GTP hydrolysis by the GTPase-activating proteins p190, p50RhoGAP, Bcr, and 3BP-1. *Biochemistry*, 37(15):5249–5257.
- [14] G. Berstein, J. Blank, DY Jhon, J. Exton, S. Rhee, and E. Ross. Phospholipase C-beta 1 is a GTPase-activating protein for Gq/11, its physiologic regulator. *Cell*, 70:411–418, 1992.
- [15] H. Benink and W. Bement. Concentric zones of active RhoA and Cdc42 around single cell wounds. *The Journal of Cell Biology*, pages 239–439, 2005.
- [16] J. E. Guyer, D. Wheeler, and J. A. Warren. FiPy: Partial Differential Equations with Python. *Computing in Science Engineering*, 11(3):6–15, 2009.
- [17] R. Haberman. *Applied Partial Differential Equations with Fourier Series and Boundary Value Problems*. 4 edition, 2003.